Oxidant-Induced Hydride Abstraction from $[Pt(\mu\text{-}PBu^t_2)(H)(PBu^t_2H)]_2$ Yielding $[Pt_2(\mu\text{-}PBu^t_2)_2(H)(PBu^t_2H)_2]C_3(CN)_5$. Spectroscopic, Crystallographic, and Theoretical Comparison of the Structures of Two "Tautomers"

Piero Leoni,*,†,‡ Marco Pasquali,† Alessandro Fortunelli,§ Guido Germano,† and Alberto Albinati⊥

Contribution from the Dipartimento di Chimica e Chimica Industriale, Università di Pisa, Via Risorgimento 35, I-56126 Pisa, Italy, Scuola Normale Superiore, Piazza dei Cavalieri, I-56126 Pisa, Italy, Istituto di Chimica Quantistica ed Energetica Molecolare (ICQEM) del CNR, Via Risorgimento 35, I-56126 Pisa, Italy, and Istituto di Chimica Farmaceutica, Università di Milano, Viale Abruzzi 42, I-20131 Milano, Italy

Received March 19, 1998

Abstract: The platinum(II) phosphido-bridged dihydride $[Pt(\mu\text{-}PBu^t_2)(H)(PBu^t_2H)]_2$, **1**, reacts with tetracyanoethylene (TCNE) in toluene to give the charge-transfer complex **1**·TCNE, which is stable only in the solid state. By dissolving **1**·TCNE in polar solvents, electron transfer occurs rapidly, followed by loss of one of the hydrido ligands and formation of the unsaturated Pt(II)Pt(II) derivative $[Pt_2(\mu\text{-}PBu^t_2)_2(H)(PBu^t_2H)_2]^+TCNE^-$, **2a**. Recrystallization of **2a** in the air gives crystals of $[Pt_2(\mu\text{-}PBu^t_2)_2(H)(PBu^t_2H)_2]^+$ $[C_3(CN)_5]^-$, **2b**, whose structure was solved by X-ray diffraction. The same type of reaction was observed when **1** was reacted with tetracyanoquinodimethane (TCNQ), forming the analogous, structurally characterized, $TCNQ^-$ salt of cation $\mathbf{2}^+$. What happened to the hydrido ligand displaced from **1** was better seen when **1** was reacted with an equimolar amount of $[Cp_2Fe]PF_6$ as the oxidant (Cp = cyclopentadienyl). In this case we isolated a 1:1 mixture of (**2**)PF_6, **2d**, and $[Pt_2(\mu\text{-}PBu^t_2)(\mu\text{-}H)(PBu^t_2H)_3(H)]PF_6$, **3d**, the latter also known to form by the reaction of complex **1** with strong acids. According to this observation, the reaction of **1** with two equivalents of $[Cp_2Fe]PF_6$ and one of triethylamine (NEt_3) gives quantitatively $[NEt_3H]PF_6$ and **2d**. The electronic structure of cation $\mathbf{2}^+$ was also investigated by means of ab initio and density functional calculations. Ignoring the different metals, cation $\mathbf{2}^+$ can be considered a "tautomer" of the known phosphine-bridged dipalladium cation $[Pd_2(\mu\text{-}PBu^t_2)(\mu\text{-}PBu^t_2H)(PBu^t_2H)_2]^+$, $\mathbf{4}^+$. Differences and analogies between the structures of the two cations were investigated by means of spectroscopic, crystallographic, and theoretical (ab initio and density functional) analyses.

Introduction

The relevance of tetracyanoethylene (TCNE) as a reagent in both organic and organometallic chemistry is well-known.[1] Cyano groups are powerful withdrawing substituents and do not impart severe steric strain to the fragments to which they bind. Being a typical electron-deficient olefin, TCNE easily reacts with nucleophiles and gives cycloaddition reactions with other olefins or dienes. Moreover, TCNE inserts into the C−H bonds of ketones and arenes[1a] and, promptly, also in the M−H, M−C, or M−M′ bonds of organometallic species.[1b]

Even as a innocent ligand, TCNE exhibits a remarkable versatility: (a) It can bind to a metal via the C═C bond, as in $(Ph_3P)_2M(CO)Cl(TCNE)$ (M = Rh, Ir)[2] or $(Ph_3P)_2Pt(TCNE)$;[3,4] (b) it may act as a σ-donor and coordinate a metal through one or more of its nitrogen atoms, as in CpVX(TCNE) (X = Cl, Br, I, Cp = cyclopentadienyl)[5a] or $Os(S_2PR_2)_2(PPh_3)(TCNE)$;[5b] (c) it can bridge two metal centers as in the cobalt derivative $[Co(acacen)(Py)]_2(TCNE)$[6a] or, as recently reported, four Ru centers.[6b]

A high electron affinity (EA = 3.17 ± 0.2 eV)[7] makes TCNE a good oxidizing agent, which can be reduced to either $TCNE^-$ [E_{red} (0/−1) = + 0.2 V] or $TCNE^{2-}$ [E_{red} (−1/−2) = − 0.77 V].[8] TCNE reacts with weak organic or organometallic electron-donors to give strongly colored charge-transfer (CT) complexes,[9] and the influence of the solvent polarity on the amount of CT has been recognized.[10]

* To whom correspondence should be addressed. Tel: 39 050 918 209. Fax: 39 050 20237. E-mail: leoni@dcci.unipi.it.
† Università di Pisa.
‡ Scuola Normale Superiore.
§ ICQEM-CNR.
⊥ Università di Milano.

(1) (a) Fatiadi, A. J. *Synthesis* **1986**, 249. (b) Fatiadi, A. J. *Synthesis* **1987**, 959.
(2) (a) Baddley, W. H. *J. Am. Chem. Soc.* **1968**, *90*, 3705. (b) Haga, M. A.; Kawakami, K.; Tanaka, T. *Inorg. Chem.* **1976**, *15*, 1946.
(3) Baddley, W. H.; Venanzi, L. M. *Inorg. Chem.* **1966**, *5*, 33.
(4) Panattoni, C.; Bombieri, G.; Belluco, U.; Baddley, W. H. *J. Am. Chem. Soc.* **1968**, *90*, 798.
(5) (a) Rettig, M. F.; Wing, R. M. *Inorg. Chem.* **1969**, *8*, 2685. (b) McQeen, A. E. D.; Blake, A. J.; Stephenson, T. A.; Schröder, M.; Yellowlees, L. J. *J. Chem. Soc., Chem. Commun.* **1988**, 1533.
(6) (a) Crumblis, A. L.; Basolo, F. *Inorg. Chem.* **1971**, *10*, 1676. (b) Moscherosch, M.; Waldhör, E.; Binder, H.; Kaim, W.; Fiedler, J. *Inorg. Chem.* **1995**, *34*, 4326.
(7) Chowdhury, S.; Kebarle, P. *J. Am. Chem. Soc.* **1986**, *108*, 5453.
(8) Olbrich-Deussner, B.; Kaim, W.; Gross-Lannert, R. *Inorg. Chem.* **1989**, *28*, 3113.

S0002-7863(98)00932-9 CCC: $15.00
Published on Web 09/05/1998

The isolation of the ionic derivatives $[D]^{n+}TCNE^{n-}$ ($n = 1$, 2) has allowed accurate studies of their structural and magnetic properties; to this respect, metallocenium derivatives have been extensively investigated and the structures of $[Cp^*_2Fe^+](TCNE^-)$ ($TCNE^-$: D_{2h})[10a] and $[Cp^*_2Co^+]_2(TCNE^{2-})$ ($TCNE^{2-}$: D_{2d})[10b] have been reported.

Electron transfer is often the first of a series of steps, and the overall reaction ends with either the coordination of TCNE or its insertion into M−H or M−C bonds.[1b] Other possible reactions stem from the destabilization of the metal complex induced by oxidation; for example, as is well established, the acidity of metal-hydrides[11] or molecular hydrogen complexes[12] can increase by several orders of magnitude when the metal is oxidized.

We report here the reaction of [Pt(μ-PBu$^t_2$)(H)(PBu$^t_2$H)]$_2$, **1**,[13] with TCNE, or other oxidants such as tetracyanoquinodimethane (TCNQ) or $[Cp_2Fe]PF_6$, yielding the new unsaturated cation $[Pt_2(\mu\text{-PBu}^t_2)_2(H)(PBu^t_2H)_2]^+$, $\mathbf{2}^+$, which is formally obtained from the abstraction of a hydride ligand from complex **1**. As shown by the crystallographic analysis of the $C_3(CN)_5^-$ and $TCNQ^-$ salts, the molecular structure of cation $\mathbf{2}^+$ is very similar to that of the known dipalladium cation $[Pd_2(\mu\text{-PBu}^t_2)(\mu\text{-PBu}^t_2H)(PBu^t_2H)_2]^+$, $\mathbf{4}^+$.[14] Cations $\mathbf{2}^+$ and $\mathbf{4}^+$, however, differ significantly in the position of a single proton, which is terminally bonded to a platinum center in cation $\mathbf{2}^+$ but bridges a palladium−phosphorus bond in cation $\mathbf{4}^+$; this difference in the bonding mode is clearly reflected in the striking differences between their solution and solid-state NMR spectra and has been confirmed by a theoretical (ab initio and density functional) study.

Results and Discussion

We recently reported the synthesis of the bis-phosphido-bridged platinum(II) derivative [Pt(μ-PBu$^t_2$)(H)(PBu$^t_2$H)]$_2$, **1**.[13] During our studies on the possibility of inserting multiple bonds into Pt−H bonds, we reacted complex **1** with TCNE and observed a very fast, strongly solvent-dependent reaction. By reacting a toluene suspension of the colorless **1** with TCNE, a deep violet solid, highly insoluble in apolar solvents and air sensitive, was isolated. The IR spectrum of this solid shows absorptions at 2289 (ν_{PtH}) and 2031(ν_{PtH}) cm^{-1}, the same as found in **1** (2289 and 2032 cm^{-1}, respectively).[13] The two spectra are nearly superimposable except for the new absorptions at 2189, 2174, 2161, and 2145 cm^{-1} (ν_{CN}), which are shifted to lower frequencies with respect to ν_{CN} in free TCNE (2260, 2247, 2235, and 2228 cm^{-1}).[10] Literature data report only two ν_{CN} absorptions for both $TCNE^-$ and $TCNE^{2-}$ (at 2144, 2138 and 2069, 2140 cm^{-1}, respectively).[10]

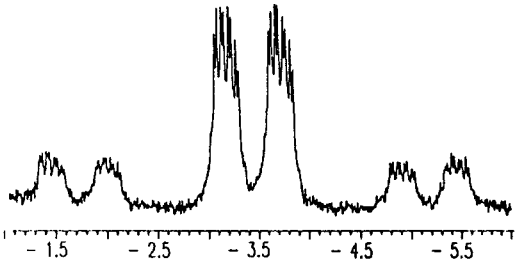

Figure 1. High-field region of the ^1H NMR spectrum ($CDCl_3$, 293 K) of **2a**.

From the presence of slightly shifted absorptions of both the reactants, we supposed the solid to be the CT complex **1**·TCNE. This hypothesis was confirmed by the results of the elemental and magnetic analyses. The solid is indeed paramagnetic by less than one (0.8) electron ($\mu_{eff} = 1.46\ \mu_B$), which, on the assumption that $\mathbf{1}^+$·$TCNE^-$ has two unpaired electrons, corresponds to ∼40% of electron transfer.

By reaction with TCNE in tetrahydrofuran (THF) as the solvent, the colorless suspension of complex **1** turned immediately to a suspension of a deep red solid, which slowly dissolved, leaving an orange solution. After workup an orange solid, identified as $[Pt_2(\mu\text{-PBu}^t_2)_2(H)(PBu^t_2H)_2]^+TCNE^-$, **2a** (eq 1), was isolated in high yield.

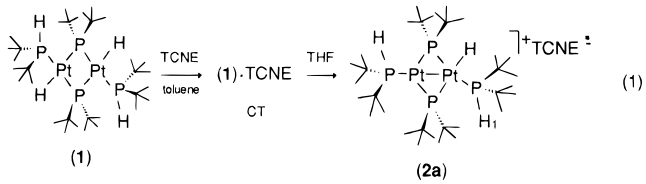

(1)

By dissolving the violet CT complex **1**·TCNE in THF, some precipitation of **1** was observed, while the $^{31}P\{^1H\}$ NMR spectrum of the solution was identical to that observed for complex **2a**. This suggests that **1**·TCNE is an intermediate in the formation of **2a**, and, indeed, in the very early steps of the reaction in THF, we occasionally observed the appearance of a violet solid, which rapidly turned red and slowly dissolved as described above.

The structure of cation $\mathbf{2}^+$ was inferred by the NMR parameters extracted from the ^1H (Figure 1), ^{31}P (Figure 2), and ^{195}Pt (Figure 3) spectra and summarized in the table shown in Figure 3. The main feature of the NMR spectra are the following: (a) a hydride signal at $\delta_H = -3.4$ ppm coupled with four nonequivalent P atoms and with the adjacent Pt center (Figure 1); (b) two low field signals at $\delta_P = 329.5$ and 348.0 ppm for the bridging P nuclei (Figure 2a), both with two different sets of satellites arising from the coupling with two inequivalent platinum centers, and two high field resonances at $\delta_P = 30.3$ and 57.5 ppm for the terminally bonded secondary phosphines (Figure 2b); (c) two signals (Figure 3a and b) at δ_{Pt}, −5586 (Pt_2) and −6268 ppm (Pt_1), the latter being split in the proton-coupled spectrum (Figure 3c) owing to the large coupling with the hydride ligand ($^1J_{PtH} = 690$ Hz).

A detailed analysis of the spectra is given in the Supporting Information.

The IR spectrum (Nujol, KBr) of the complex shows significant absorptions at 2188 and 2159 cm^{-1}, which may be assigned to the ν_{CN} of the $TCNE^-$ moiety, and at 2039 cm^{-1}, which may be from the ν_{Pt-H} stretch. The magnetic measurements suggest one unpaired electron ($\mu_{eff} = 1.62\ \mu_B$). Since

(9) Brandon, R. L.; Osiecki, J. H.; Ottenberg, A. *J. Org. Chem.* **1966**, *31*, 1214.

(10) (a) Miller, J. S.; Calabrese, J. C.; Rommelmann, H.; Chittipeddi, S. R.; Zhang, J. H.; Reiff, W. M.; Epstein, A. J. *J. Am. Chem. Soc.* **1987**, *109*, 769. (b) Dixon, D. A.; Miller, J. S. *J. Am. Chem. Soc.* **1987**, *109*, 3656.

(11) (a) Ryan, D. B.; Tilset, M.; Parker, V. D. *J. Am. Chem. Soc.* **1990**, *112*, 2618. (b) Ryan, D. B.; Tilset, M.; Parker, V. D. *Organometallics* **1991**, *10*, 298. (c) Costello, M. T.; Walton, R. A. *Inorg. Chem.* **1988**, *27*, 2563. (d) Zlota, A. A.; Tilset, M.; Caulton, K. G. *Inorg. Chem.* **1993**, *32*, 3816. (e) Hamon, P.; Hamon, J.-R.; Lapinte, C. *J. Chem. Soc., Chem. Commun.* **1992**, 1602.

(12) (a) Zanello, P. *Comments Inorg. Chem.* **1991**, *11*, 339. (b) Harman, C. D.; Taube, H. *J. Am. Chem. Soc.* **1990**, *112*, 2261. (c) Bianchini, C.; Laschi, F.; Peruzzini, M.; Ottaviani, F. M.; Vacca, A.; Zanello, P. *Inorg. Chem.* **1990**, *29*, 3394.

(13) Leoni, P.; Manetti, S.; Pasquali, M. *Inorg. Chem.* **1995**, *34*, 749.

(14) (a) Leoni, P.; Pasquali, M.; Sommovigo, M.; Laschi, F.; Zanello, P.; Albinati, A.; Lianza, F.; Pregosin, P. S.; Rüegger, H. *Organometallics* **1993**, *12*, 1702. (b) Albinati, A.; Lianza, F.; Pasquali, M.; Sommovigo, M.; Leoni, P.; Pregosin, P. S.; Rüegger, H. *Inorg. Chem.* **1991**, *30*, 4690. (c) The cations $\mathbf{2}^+$ and $\mathbf{4}^+$ can be obtained through the protonation of the corresponding neutral derivatives [M(μ-PBu$^t_2$)(PBu$^t_2$H)]$_2$. This was shown[14a,b] for M = Pd and will be reported in a future paper for M = Pt.

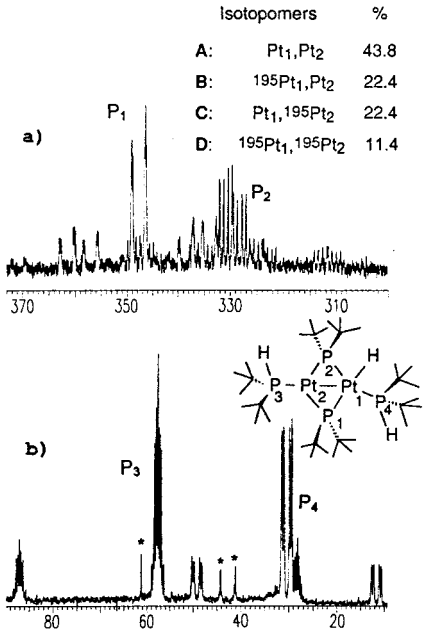

Figure 2. $^{31}P\{^1H\}$ NMR spectrum ($CDCl_3$, 293 K) of **2a** with labeling scheme and table of the isotopomers' [51] ratio. The peaks marked (*) are from an impurity.

the cation contains two Pt(II)Pt(II) centers and is diamagnetic, the paramagnetism is likely to be attributable only to the radical anion $TCNE^-$. Moreover, this radical anion is remote from the coordination spheres of the platinum centers, as suggested by the well-resolved NMR signals and by the UV−Vis spectrum, which shows the typical absorption of free $TCNE^-$ at 23375 cm^{-1} with a fine structure given by vibrational overtones[10] (the dianion $TCNE^{2-}$ gives a well separated maximum at 44450 cm^{-1} without fine structure).[10b]

The overall reaction can thus be seen as the abstraction of one of the hydride ligands from **1**, which yields the electronically unsaturated $Pt^{II}Pt^{II}$ cation $\mathbf{2}^+$, containing a 14 e^- platinum center (eq 1). Accordingly, the hydride, and not one of the platinum atoms, is the nucleus eventually oxidized. Gas-chromatographic analysis of the gas phase, at the end of the reaction, did not reveal the presence of molecular hydrogen. Note that, to be completed, this reaction requires at least two equivalents of TCNE and, when the CT complex **1**·TCNE is isolated and dissolved in polar solvents, its transformation into **2a** is always accompanied by the precipitation of significant amounts of complex **1**.

These results strongly suggest that the reaction requires an overall two-electron oxidation, and, as will be clearer in the reaction of **1** with $[Cp_2Fe]^+$ (see below), the hydride is probably oxidized to H^+.

The structure of the cation $\mathbf{2}^+$ has been confirmed by a crystallographic study (discussed below). Recrystallization of a sample of **2a** from acetone−diethyl ether (Et_2O) mixtures in air gives, with low yields, single crystals of **2b** containing [by $^{31}P\{^1H\}$ NMR] the cation $\mathbf{2}^+$ and the pentacyanoallyl moiety $[C_3(CN)_5^-]$ as counterion, possibly resulting from the reaction of $TCNE^-$ with O_2 and H_2O.[15]

The first steps of the reaction of eq 1 present some analogies with the insertion of TCNE into the M−H or M−C bonds of group 14 hydrides or alkyls studied by Kochi and co-workers;[16] these reactions proceed through the formation of the CT complex [D]·TCNE (D = R_3MR'; M = Si, Ge, Sn; R′ = H, alkyl), electron transfer to $[D]^+TCNE^-$, and $TCNE^-$ insertion into the M−H or M−alkyl bonds. In our system, $TCNE^-$ does not insert into one of the Pt−H bonds of complex **1**, probably because of the large steric hindrance of the eight *tert*-butyl substituents. This may also explain why the $TCNE^-$ anion does not coordinate to the electronically unsaturated platinum center in **2a**.

Reaction of Complex 1 with TCNQ. As in the reaction with TCNE, complex **1** reacts with TCNQ to give **2c**,[15c] the $TCNQ^-$ salt of cation $\mathbf{2}^+$. In this case we could not isolate the intermediate CT complex **1**·TCNQ. Complex **2c** gives ^{31}P and ^1H NMR spectra superimposable with the corresponding spectra of **2a** and **2b**; the resonances of the protons of the $TCNQ^-$ radical anion were not observed in the ^1H NMR spectrum, presumably because of severe broadening. As expected, complex **2c** is paramagnetic by one electron ($\mu_{eff} = 1.82\ \mu_B$).

Reaction with $[Cp_2Fe]PF_6$. Further details on the reaction of **1** with oxidants were obtained by investigating the reaction with $[Cp_2Fe]PF_6$, which allowed us to clarify the fate of the hydrido ligand abstracted from **1**. Equimolar amounts of **1** and $[Cp_2Fe]PF_6$ were suspended in toluene and stirred for a few hours at 50 °C. After workup, a 1:1 mixture of **2d**, and $[Pt_2\{\mu\text{-}P(t\text{-}Bu)_2\}(\mu\text{-}H)\{P(t\text{-}Bu)_2H\}_3(H)]^+PF_6^-$, **3d**, was isolated (eq 2).

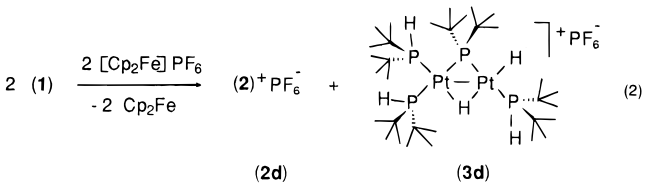

The $^{31}P\{^1H\}$ NMR spectrum of this mixture shows all the resonances of the cations $\mathbf{2}^+$ and $\mathbf{3}^+$ [13] and the PF_6^- septet at −139 ppm ($^1J_{PF} = 708$ Hz). We have previously reported the nearly quantitative conversion of complex **1** into (**3**)BF_4 by reaction with HBF_4;[13] the result of eq 2 strongly supports the hypotheses that the hydride removed from **1** is oxidized to H^+, which, in turn, protonates half of the reagent. As expected, when the reaction is performed in the presence of triethylamine (Et_3N), which removes the acid, the formation of **2d** is quantitative (eq 3); obviously, in this case, two equivalents of ferricinium per equivalent of **1** must be used.

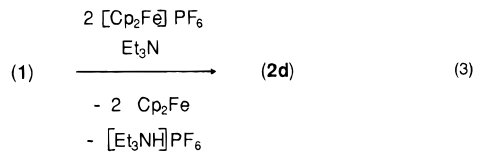

The reactions of eqs 2 and 3 can proceed through various alternative elementary steps.[17] Unfortunately, an electrochemical investigation, the most likely method to help in discriminating which paths were actually taken, was prevented by the extremely low solubility of complex **1**. We did, however, definitively confirm that the overall reaction is a bi-electronic oxidation of the Pt(II)Pt(II) complex **1**, forming H^+ and $\mathbf{2}^+$ and

(15) (a) Wanzlick, H.-W.; Lachmann, B. *Z. Naturforschung.* **1969**, *24B*, 574. (b) Giraudon, J. M.; Sala-Pala, J.; Guerchais, J. E.; Toupet, L. *Inorg. Chem.* **1991**, *30*, 891. (c) Complexes **2a**−**d** contain the same cation ($\mathbf{2}^+$) and different anions: **2a** = $(\mathbf{2})^+TCNE^-$, **2b** = $(\mathbf{2})^+[C_3(CN)_5]^-$, **2c** = $(\mathbf{2})^+TCNQ^-$, **2d** = $(\mathbf{2})^+PF_6^-$.

(16) (a) Klingler, R. J.; Mochida, K.; Kochi, J. K. *J. Am. Chem. Soc.* **1979**, *101*, 6626. (b) Fukuzumi, S.; Mochida, K.; Kochi, J. K. *J. Am. Chem. Soc.* **1979**, *101*, 5961. (c) Fukuzumi, S.; Wong, C. L.; Kochi, J. K. *J. Am. Chem. Soc.* **1980**, *102*, 2928.

(17) Quadrelli, E. A.; Kraatz, H.-B.; Poli, R. *Inorg. Chem.* **1996**, *35*, 5154; and references therein.

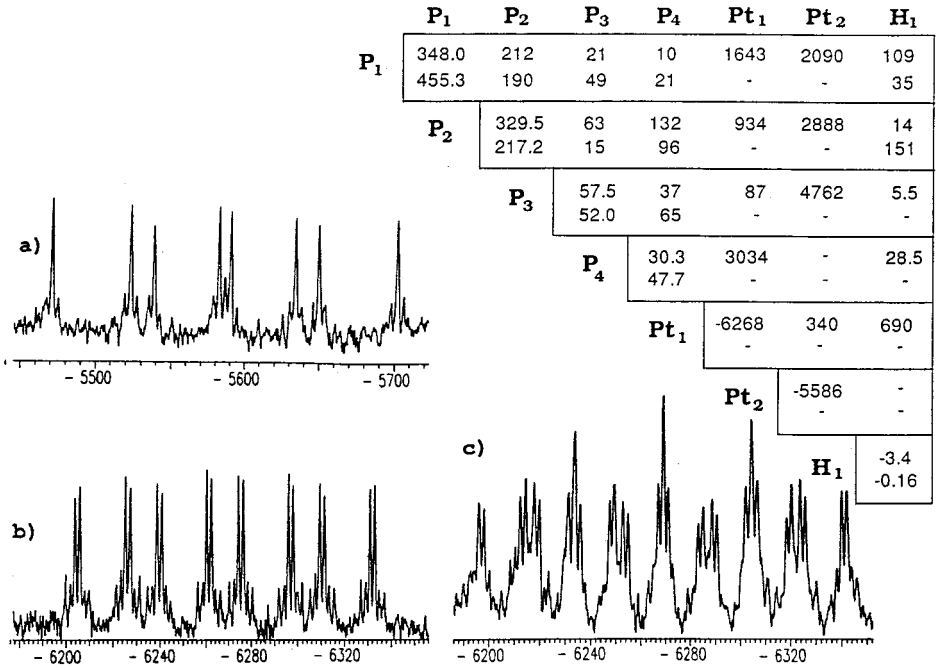

	P_1	P_2	P_3	P_4	Pt_1	Pt_2	H_1
P_1	348.0 455.3	212 190	21 49	10 21	1643 -	2090 -	109 35
P_2		329.5 217.2	63 15	132 96	934 -	2888 -	14 151
P_3			57.5 52.0	37 65	87 -	4762 -	5.5 -
P_4				30.3 47.7	3034 -	- -	28.5 -
Pt_1					-6268 -	340 -	690 -
Pt_2						-5586 -	- -
H_1							-3.4 -0.16

Figure 3. ^{195}Pt{^{1}H} NMR spectrum ($CDCl_3$, 293 K) of **2a**: (a) Pt_1, (b) Pt_2, (c) Pt_2 in the proton decoupled spectrum. The table summarizes NMR parameters from ^{1}H, ^{31}P, and ^{195}Pt NMR spectra of cations $\mathbf{2}^+$ (upper values) and $\mathbf{4}^+$ (lower values).

leaving the platinum centers still in the +II oxidation state: formally, the reaction provides the oxidation of H^- to H^+.

Moreover, we can exclude that the reaction occurs, as in eq 4, through the previous dissociation of a hydride.

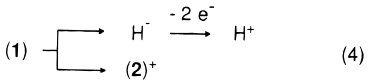

(4)

If **1** could predissociate one of the hydride ligands, as in eq 4, it would probably have also given cation $\mathbf{2}^+$ (and molecular hydrogen) in the reaction with strong acids (eq 5, right side). As already anticipated, however, this is not the case, and complex **1** is protonated by HBF_4 to give complex (**3**)BF_4 in nearly quantitative yield (eq 5, left side).

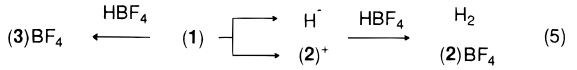

(5)

The oxidation of transition metal hydrides, followed by proton transfer, has precedents in the literature.[11] As recently surveyed in an elegant of work by Poli and co-workers,[17] the oxidation process is generally followed by deprotonation, which may be effected by either an added base or the metal hydride reagent, with consumption of either 2 or 1 faraday of oxidant per mole of M−H, respectively.

Our system behaves similarly in the first steps of the reaction and becomes somewhat more complicated in the absence of an external base, when complex **1** acts as the proton acceptor. As shown previously,[13] complex **1** is protonated at the phosphorus and not at the metal (or at one hydride). The number of hydride ligands remains therefore unchanged and the protonation, as often happens to metal monohydrides, ends up with a cationic metal dihydride. The latter are frequently unstable toward reductive elimination of H_2 but sometimes may be stable, especially with the more basic 5d metals that form the stronger M−H bonds and favor the formation of classical polyhydrides.[17] This is the case for cation $\mathbf{3}^+$, where the reductive elimination of H_2 is further hampered by the trans disposition of the two hydride ligands.

Solvent Effects. We have shown above that the reaction from **1** to $\mathbf{2}^+$ proceeds through an overall bi-electronic oxidation and a proton-transfer step.

In the absence of stronger bases, the proton released after the oxidation of **1** attacks the strongest base found in toluene solution, complex **1** itself, to form $\mathbf{3}^+$. However, complex **1** is a very weak base; indeed, when the basicity of the medium was enhanced, by using THF as the solvent, no trace of $\mathbf{3}^+$ was observed. When the ratio **1**/$[Cp_2Fe]PF_6$ was equimolar, one-half equivalent of **1** was quantitatively transformed into $\mathbf{2}^+$, leaving one-half equivalent of unreacted **1**. The reaction went to completion with a twofold excess of ferricinium, the same behavior observed in the toluene/Et_3N system.

As Quadrelli et al. emphasized,[17] adventitious water, more basic than THF, could play an important role. However, we observed no significant differences between the reactions conducted in wet or in strictly anhydrous conditions.

These data somehow account for the analogous solvent effect observed in the reaction of **1** with TCNE, which gives **1**·TCNE in toluene and **2a** in THF.

What seems, at first sight, rather puzzling is why the reaction stops in toluene at the CT complex **1**·TCNE and does not proceed further to a 1:1 mixture of the $TCNE^-$ salts of $\mathbf{2}^+$ and $\mathbf{3}^+$. A reasonable explanation may be the extremely low solubility of both **1**·TCNE and **1**, which should act as the proton acceptor in toluene. Alternatively (or concurrently), one must take into account of the lower reduction potential of TCNE ($E^\circ = -0.27$ V vs $[Cp_2Fe]^+$).[18]

Crystal Structures of [Pt$_2$(μ-PBu$^t_2$)$_2$(H)(PBu$^t_2$H)$_2$][C$_3$(CN)$_5$], 2b, and [Pt$_2$(μ-PBu$^t_2$)$_2$(H)(PBu$^t_2$H)$_2$][TCNQ], 2c. An Oak Ridge thermal ellipsoid plot (ORTEP) view of the cation $\mathbf{2}^+$ is given in Figure 4, and a selection of relevant bond lengths and angles is listed in Table 1. The full numbering scheme for both structures is given in the Supporting Information.

(18) Connelly, N. G.; Geiger, W. E. *Chem. Rev.* **1996**, *96*, 877.

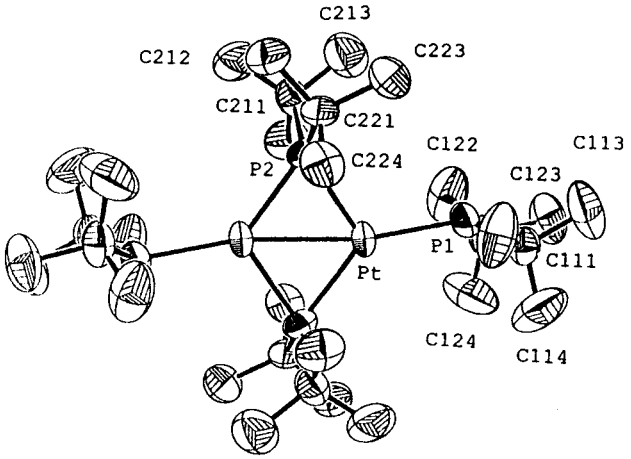

Figure 4. ORTEP view of cation $\mathbf{2}^+$ (thermal ellipsoids are at 70% probability, hydrogens are omitted for clarity).

Table 1. Selected Bond Distances (Å) and Angles (deg) for **2b**, **2c**, and cation $\mathbf{4}^+$

	2b (M = Pt)	**2c** (M = Pt)	$\mathbf{4}^{+a}$ (M = Pd)
	Bond Distances, Å		
M1−M1′[b]	2.6473 (5)	2.655 (1)	2.611 (1)
M1−P1	2.272 (2)	2.217 (9)	2.327 (4)
M1−P2	2.310 (2)	2.281 (6)	2.392 (1)
M1−P2′	2.318 (2)	2.311 (7)	2.327 (4)
C−C[a]	1.43 (2)	1.42 (8)	
C−N[a]	1.11 (4)	1.13 (2)	
	Bond Angles, deg		
M1−P2−M1′	69.77 (6)	70.6 (2)	67.4 (1)
M1−M1′−P1	168.69 (6)	169.7 (3)	170.7 (7)
P1−M1−P2	113.45 (8)	114.5 (3)	113.0 (8)
P1−M1−P2′	136.32 (7)	136.1 (3)	134.4 (7)
P2−M1−P2′	110.23 (6)	109.4 (2)	112.1 (7)
M1−P1−C111	115.2 (3)	119 (1)	115.5 (3)
M1−P1−C121	113.7 (2)	118 (1)	115.5 (6)
M1−P2−C211	118.5 (3)	119.3 (9)	119 (2)
M1−P2−C221	115.7 (3)	116.2 (7)	116.7 (5)
C1−C2−C1′	131 (2)		
C2−C1−C5	122 (2)		
C2−C1−C4	120 (2)		
C1−C5−N[a]	172 (3)	176 (3)	

[a] Average values: the esd on the average is obtained as esd = $[(N-1)^{-1}\sum(x_i-\bar{x})^2]^{1/2}$ for cation $\mathbf{4}^+$ the average is over the two independent molecules in the unit cell.[14] Esd's for the last significant digit are given in parentheses. [b] Primed atoms are obtained from those unprimed by the following symmetry operations: $-x, -y, 1-z$ for **2c** and $\mathbf{4}^+$; $-1/_2 - x, 1/_2 - y, -z$ for **2b**.

The geometry of the cation $\mathbf{2}^+$ is very similar in both structures and comparable with that found in $[Pd_2(\mu\text{-}PBu^t_2)(\mu\text{-}PBu^t_2H)(PBu^t_2H)_2]^+$, $\mathbf{4}^+$.[14a,b]

In compounds **2a** and **2b** the cations $\mathbf{2}^+$ sit on a crystallographic symmetry element; and only half of the molecules are thus independent. This situation is similar to that found in $\mathbf{4}^+$: The crystallographic symmetry does not correspond to the molecular symmetry. In both **2b** and **2c**, the cation $\mathbf{2}^+$ is pseudo-symmetric and the presence of the crystallographic symmetry implies that the coordination sphere around each metal must be identical. However, this is clearly contradicted by solution and solid-state (see next section) NMR spectra, and the solid-state structures should therefore be considered as resulting from an averaged disordered situation obtained by superimposing two molecules, each having two different Pt environments, across the symmetry elements and cannot be used to obtain insight into the nature of the bonding mode of the hydride.

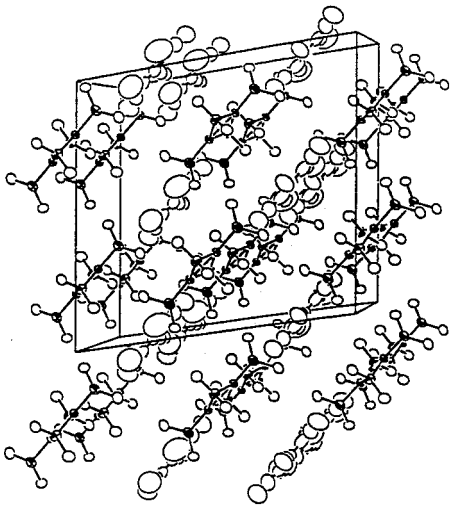

Figure 5. Perspective view of the crystal packing of **2b** normal to (010).

It was impossible to locate the hydrido ligand, bound to the platinum centers, in both compounds (see experimental). However, the distortions of the bond angles around the Pt atoms in **2b** and **2c**, e.g., P1−Pt−P2 averaging 114.0 (7)° and P1−Pt−P2′ averaging 136.2 (1)°, are indicative of the presence of the hydrido ligand.[14b]

The Pt−Pt distances in **2b** and **2c** are very similar and fall in the expected range.[14a,19] The small difference (see Table 1) may be ascribed to the different molecular environments caused by the different packing in the two compounds.

Because the metal−metal bond in $\mathbf{4}^+$ [2.611(1) Å] is shorter than in **2b** and **2c** [2.6473(5) and 2.655(1) Å, respectively] the Pd−P−Pd angle in $\mathbf{4}^+$ [67.4(1)°] is more acute than that found in the platinum complexes (av. 70.2°). Moreover, in $\mathbf{4}^+$, the two Pd−P2 distances are very asymmetric (av. 2.392(1) and 2.327(4) Å), a pattern consistent with the presence of a Pd−H−P moiety; in $\mathbf{2}^+$, the asymmetry on the Pt−P2 bonds is much less pronounced: 0.030(7) Å in **2c** and 0.008(2) Å in **2b**. This, also, is consistent with the presence of a different type of metal−hydride interaction, which will be discussed in the following sections.

The $[C_3(CN)_5]^-$ ion in **2b** has an imposed crystallographic symmetry and thus only half of it is independent. The bond distances and angles are unexceptional and similar to those already reported in the literature.[10a]

In **2c** the $TCNQ^-$ anion is located across an inversion center with bond distances and angles in the expected range; however, the poor accuracy of the determination prevents any further discussion of this arrangement.

The packing in **2b** and **2c** is very different, as shown in Figure 5 and Figure 6. In the former, the anion and cations forms parallel alternating layers; in the latter, this stacking is absent.

Comparison of the structures of two "tautomers". If we set aside the different metals, Pt and Pd, the two cations $\mathbf{2}^+$ and $\mathbf{4}^+$ may be considered as "tautomers", differing only in the position of a single hydrogen atom. Therefore, we may view the two structures as two snapshots of the system—just before ($\mathbf{4}^+$) and just after ($\mathbf{2}^+$) the oxidative addition of a P−H bond. A small structural rearrangement, a single proton that moves toward the phosphorus atom, lengthens the bond with the metal and causes major electronic effects. How significantly different are the two structures is clearly shown by their $^{31}P\{^1H\}$ NMR

(19) Leoni, P.; Pasquali, M.; Sommovigo, M.; Albinati, A.; Pregosin, P. S.; Rüegger, H. *Organometallics* **1996** *15*, 2047.

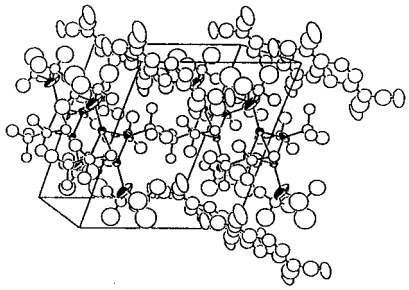

Figure 6. Perspective view of the crystal packing of **2c** normal to (100).

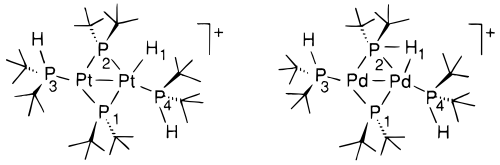

(**2**)$^+$ (**4**)$^+$

solution spectra. The cation **2**$^+$ has four ^{31}P signals, two at high fields (30.3 and 57.5 ppm) for the terminally bonded secondary phosphines, and two for the bridging phosphido ligands at very low fields (329.5 and 348.0 ppm). The corresponding spectrum of the cation **4**$^+$ shows two high field signals (at 47.7 and 52.0 ppm) for the terminal phosphines, one at low fields (217 ppm) for the bridging phosphine, and one at very low fields (455 ppm) for the bridging phosphido. The latter two signals, whose analogues were nearly superimposed in **2**$^+$, are separated by ∼240 ppm in **4**$^+$. Moreover, an M−H stretching absorption observed in the IR (Nujol) spectrum of (**2**)PF_6 at 2039 cm^{-1} is lacking in the corresponding spectrum of (**4**)BF_4.

Contrary to this outstanding difference in the solution NMR spectra and the solid-state IR spectra, the single crystal molecular structures of the two cations are nearly superimposable (see Figure 8 in the next section), notwithstanding the different metals involved.

While we had no doubt that **4**$^+$ retains the solution structure also in the solid state [its single pulse excitation/magic-angle spinning (SPE/MAS) ^{31}P{^{1}H} NMR spectrum is similar to the corresponding solution spectrum],[14a] we were not sure whether the same was true for **2**$^+$.

Actually, the solid-state ^{31}P{^{1}H} NMR spectrum of **2d** is complicated by the spinning sidebands of the bridging P_1 and P_2; given the great anisotropy of these resonances, a relatively clean spectrum was obtained only at a high spinning rate (15 kHz). The expected four signals were clearly identified by varying the spinning rate at 359, 329, 55, and 29 ppm (Figure 7), practically in the same positions of the solution spectra. Although the line broadening obscures the PP couplings, the PPt couplings manifest themselves with broad satellites that roughly give the same J_{PPt} values as are found in solution.

The appearance of the solid-state ^{31}P{^{1}H} NMR spectrum clearly shows that the solution structure of cation **2**$^+$ is retained in the solid state.

Additional information was given by the cross-polarization/magic-angle spinning (CP/MAS) ^{31}P{^{1}H} NMR spectrum of **2d**, which shows that a significant amount of magnetization is transferred to the bridging phosphorus P_2, which is cis to the hydride. This could be explained either by a direct H_1-P_2 bond interaction, as in **4**$^+$, or by a dipolar through-space interaction, stemming from the proximity imposed by the cis-disposition of the two nuclei. Although this evidence is not very informative in itself, it becomes significant in a more general context.

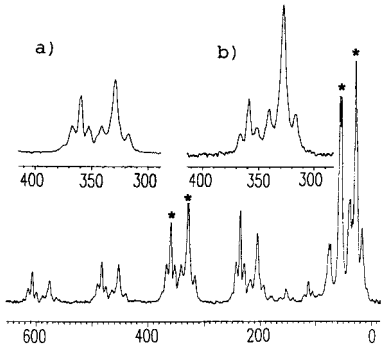

Figure 7. Solid-state SPE-MAS ^{31}P{^{1}H} NMR spectrum (sample rotation = 15 kHz, T = 300 K) of (**2**)PF_6; isotropic signals are marked with an asterisk (*); (a) enlargement of the signals from the bridging phosphides; (b) CP/MAS spectrum.

Chart 1

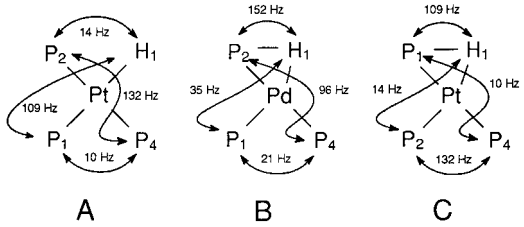

We can in fact observe that the coupling of H_1 to P_2 (to which the magnetization is transferred) is much smaller than the coupling to the other bridging phosphorus P_1 ($^2J_{P2H1}$ = 14, $^2J_{P1H1}$ = 109 Hz: **A** in Chart 1). This is in good agreement with the structure **2**$^+$, where H_1 is trans to P_1 and cis to P_2. In the cation **4**$^+$, polarization transfer to P_2 is accompanied by the opposite trend in the coupling constants: a large coupling to P_2, $^1J_{P2H1}$ = 152 Hz, because of the partial H_1-P_2 bond interaction, and a small coupling to P_1, $^2J_{P1H1}$ = 35 Hz (**B** in Chart 1). This discrepancy would deceptively be overcome by reversing the attribution of the signals assigned to P_1 and P_2 in **2**$^+$ (**C** in Chart 1), but this would give meaningless values of $^2J_{P4P1,2}$. The large value of $^2J_{P4P2}$ (132 Hz) and the small value of $^2J_{P4P1}$ (10 Hz) are in fact fully consistent with the former assignment (**A**, with P_4 trans to P_2 and cis to P_1) and harshly contrast with the reverse (**C**).

On the other hand, **A** and **C** are only extreme descriptions of the bonding situation, and some P2−H1 interaction in **2**$^+$, much weaker than the corresponding interaction in **4**$^+$, cannot be ruled out completely.[20]

To gain further insight, we performed a theoretical investigation to elucidate the nature of the P··H··M (M = Pd, Pt) interactions in the "tautomer" cations **2**$^+$ and **4**$^+$.

Theoretical Analysis

The first problem we addressed was the localization of the H_1 atom with respect to P_2 and Pt_1 or Pd_1 (using the same notation as in patterns **A** and **B** of Chart 1 above). Given the complexity of these cations, the *tert*-butyl groups were replaced by methyl groups: this should not alter the description of the "core" region of the compounds. Thus, all the P, Pt, Pd, and C(−P) atoms were kept at their crystallographic positions, taken

(20) Some P_2-H_1 interaction could be suggested by (a) the absence of a trans-effect of the hydride ligand (see Table 1) in the Pt−P (bridging) distances (however, bond distances in these cations could be influenced by the large steric strain induced by eight adjacent *tert*-butyl substituents bound to a small four-membered ring, and by the pseudosymmetry); (b) the lower value of $^1J_{P2Pt1}$ (943 Hz) in comparison with other Pμ−Pt couplings (1643, 2090, and 2888 Hz).

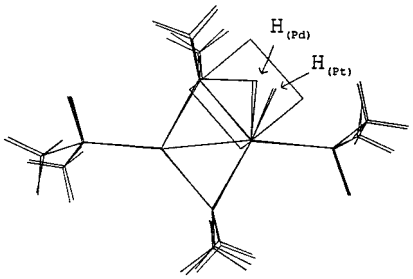

Figure 8. Superposed structures of the cations $\mathbf{2}^+$ and $\mathbf{4}^+$, top view. The square shows the region where the total electron density was computed. HF and DF place H_1 in two slightly different positions (closer to P_2, according to HF).

Table 2. Optimized Distances (Å)

	HF		DF	
M	H_1-M_1	H_1-P_2	H_1-M_1	H_1-P_2
Pd	1.785	1.551	1.792	1.668
Pt	1.644	2.107	1.675	2.189

from our previous work[14] for $\mathbf{4}^+$ and from the present work for $\mathbf{2}^+$. The positions of three hydrogen atoms (the P−H's and H_1) were then fully optimized in first principle calculations. Hartree−Fock (HF) and DF approaches were utilized, with the DF approach using the functional of Becke[21] for exchange and that of Lee−Yang−Parr [22] for correlation. In all cases, a stable energy minimum was found for the H_1 atom in the $P_2-M_1-P_4$ plane. The optimized bond distances for the four possible combinations of systems [$\mathbf{2}^+/\mathbf{4}^+$] and methodologies of calculation (HF/DF) are shown in Table 2 and Figure 8.

A major difference between the Pd and the Pt case follows immediately from a brief inspection of these results: in the Pt case, H_1 is closer to Pt_1 than to P_2, whereas in the Pd case, H_1 is about halfway between Pd_1 and P_2, slightly closer to the latter. It thus seems that in the Pt case, H_1 is substantially bound only to the metal center, exhibiting weak interactions with the phosphido ligand, whereas in the Pd case, H_1 seems to interact with both centers, slightly more with P_2 than with Pd_1; this result is given by both the HF and DF calculations. A thorough scan of the potential energy surface of the H_1 atom in the $P_2-M_1-P_4$ plane, performed in all four cases, excluded the presence of potential double-wells: We found that each energy minimum corresponded to a stable and unique configuration. Shifting the hydrogen from its minimum position to that for the other metal, the HF (and DF) energy increased by 10.4 (3.9) kcal/mol for M = Pd and by 10.3 (8.1) kcal/mol for M = Pt. The smaller DF energy difference for Pd is consistent with a picture of a rather symmetric three-center ($Pd_1-H_1-P_2$) interaction, the stretching of one bond being compensated by the shortening of the other. The HF scheme allowed less compensation because, lacking correlation energy, the description of a three-center bond is problematic.

To further analyze the bonding situation, we used a Mulliken population analysis in the four cases; its results are reported in Tables 3 and 4. For comparison, the Mulliken charges and bond orders are reported also for the related conjugate bases: [M(μ-PBu$^t_2$)(PBu$^t_2$H)]$_2$, M = Pd, Pt, evaluated at the geometry of $\mathbf{2}^+/\mathbf{4}^+$. Given the well-known shortcomings of the Mulliken population analysis, we complemented this with an analysis of the total electron density between the atoms of interest, following

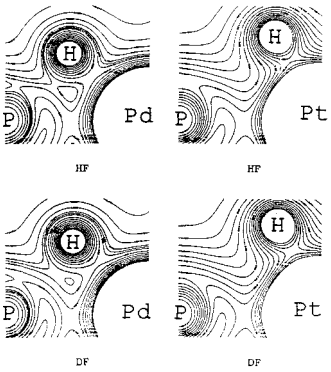

Figure 9. Contour plots of the total electron density (in a.u.) of the cations $\mathbf{2}^+$ and $\mathbf{4}^+$ in the $P_2-H_1-M_1$ plane (M = Pt, Pd). A maximum along directions roughly orthogonal to a line connecting two nuclei is a characteristic feature of a chemical bond. The density holes around the P_2 and M_1 nuclei are due to the use of pseudopotentials, which allow neglecting the core electrons in the calculations. Isodensity lines were plotted every 0.01 units, plus one extra line at 0.055 for Pd HF and one extra line at 0.045 for Pd DF, to show the local density minimum in the middle of the three nuclei.

Bader's method;[23] representative plots of this quantity in the P_2-H_1-M_1 plane are shown in Figure 9 for the four cases. From the analysis of Tables 3 and 4 and Figure 9, the following conclusions can be drawn:

(a) H_1 is more positively charged in the Pt case than in the Pd case. This conclusion is supported by the values of the Mulliken gross atomic charges on H_1 ($q_{Pd/HF} = -0.07$, $q_{Pd/DF} = 0.03$, $q_{Pt/HF} = 0.08$, $q_{Pt/DF} = 0.13$), and by the fact that the total electron density is apparently more clouded around H_1 in the Pd case (see Figure 9).

(b) Despite the changes in the bonding situation, there are no large changes in the values of the Mulliken charges on the other atoms. Even the introduction of the H^+ ion results in a drawing of charge from the external region of the complex to the "core" region and from the M_2 fragment to the M_1 fragment, finally resulting in a situation in which the metal centers exhibit a much less positive charge than the formal one.[24]

(c) Both the Mulliken and the Bader population analyses confirm the hypothesis about the $P_2-H_1-M_1$ interactions. In the Pt case, H_1 is bound substantially only to the metal with a strong bond and not to P_2, whereas in the Pd case, it is involved in a three-center $P_2-H_1-M_1$ bond.

(d) Focusing on the Mulliken analysis, we can see that electron correlation slightly lengthens the bond distances and decreases the bond orders in the Pt case, whereas the effect is more appreciable in the Pd case in which the three-center character of the $P_2-H_1-M_1$ bond is strongly enhanced to give an "equimolar" mixture of H_1-P_2 and H_1-M_1, each of which is weaker than a "pure" H−P or H−M bond, while the P_2-M_1 bond order is slightly increased. The bonding pattern is even more evident from a Bader analysis (see Figure 9), according to which a maximum of the total electron density along

(21) Becke, A. D. *Phys. Rev. A*, **1988**, *33*, 2786.
(22) Lee, C.; Yang, W.; Parr, R. G. *Phys. Rev. B* **1988**, *37*, 785.

(23) Bader, R. F. W. *Atoms in Molecules: A Quantum Theory*, Oxford University Press: Oxford, 1990.

(24) As a general remark in the analysis of Mulliken charges, relative changes between related compounds are more significant than absolute values; moreover, the absolute value of DF charges is smaller than that of HF ones, except for the Pd atoms, because the inclusion of electron correlation decreases the contribution of ionic configurations to bonds. In this regard, relativistic effects make Pt more electronegative than Pd and give it therefore a more-negative apparent charge. A full inclusion of relativistic effects would further enhance this tendency and lead to a contraction of the H−M bond length and an increase of the H−M and P−M bond orders (see, e.g., Fantucci, P.; Polezzo, S.; Sironi, M.; Bencini, A. *J. Chem. Soc., Dalton Trans.* **1995**, 4121).

Table 3. Values of the Mulliken Bond Population Analysis

	P1	P2	P3	P4	Pt1	Pt2	H	GAP[a]
P1	3.58/3.87[a] (3.67/4.00)	−	−	−	0.22[b] (0.18)	0.19 (0.25)	−	0.65/0.48 (0.61/0.45)
P2	−	3.61/3.93 (3.67/4.00)	−	−	0.18 (0.25)	0.14 (0.18)	0.07	0.67/0.49 (0.61/0.45)
P3	−	−	3.44/3.71 (3.56/3.85)	−	−	0.26 (0.25)	−	0.65/0.47 (0.62/0.43)
P4	−	−	−	3.47/3.76 (3.56/3.85)	0.18 (0.25)	−	−	0.64/0.46 (0.62/0.43)
Pt1	0.25[c] (0.24)	0.21 (0.31)	−	0.21 (0.22)	18.45/18.65 (18.21/18.41)	−0.42 (−0.32)	0.22	−0.78/−0.67 (−0.55/−0.44)
Pt2	0.26 (0.31)	0.20 (0.24)	0.25 (0.22)	−	−0.16 (−0.04)	18.18/18.43 (18.21/18.41)	−	−0.37/−0.31 (−0.55/−0.44)
H	−	0.07	−	−	0.25	−	0.63/0.61	0.08/0.13
	P1	**P2**	**P3**	**P4**	**Pd1**	**Pd2**	**H**	**GAP**
P1	3.61/3.75[a] (3.69/3.80)	−	−	−	0.27[b] (0.29)	0.23 (0.26)	−	0.63/0.51 (0.58/0.49)
P2	−	3.63/3.81 (3.69/3.80)	−	−	0.14 (0.26)	0.21 (0.29)	0.15	0.63/0.50 (0.58/0.49)
P3	−	−	3.53/3.71 (3.55/3.77)	−	−	0.27 (0.27)	−	0.61/0.46 (0.63/0.46)
P4	−	−	−	3.52/3.71 (3.55/3.77)	0.25 (0.27)	−	−	0.60/0.46 (0.63/0.46)
Pd1	0.26[c] (0.28)	0.12 (0.28)	−	0.22 (0.20)	17.98/18.01 (17.87/17.94)	−0.16 (−0.13)	0.13	−0.38/−0.44 (−0.39/−0.41)
Pd2	0.25 (0.28)	0.18 (0.28)	0.23 (0.20)	−	−0.05 (0.00)	17.81/17.87 (17.87/17.94)	−	−0.21/−0.25 (−0.39/−0.41)
H	−	0.20	−	−	0.09	−	0.87/0.75	−0.07/0.03

[a] Values on the diagonal and Gross Atomic Population (GAP) are for HF/DF. [b] Values from upper triangular region of table are from DF calculations (a.u.). [c] Values from the lower triangular region are from HF calculations. The values within parentheses are for the related compounds without the H^+ ion. See the text for the definition of the atom numbering.

Table 4. Total Electron Density (au) at the Saddle Critical Points along the Bonds

	HF			DF		
M	H_1-M_1	H_1-P_2	P_2-M_1	H_1-M_1	H_1-P_2	P_2-M_1
Pd	0.0658	0.0553	0.0634	0.0588	0.0464	0.0627
Pt	0.1188	−	0.0946	0.1148	−	0.0946

directions roughly orthogonal to a line connecting two nuclei is a characteristic feature of a chemical bond. The values of the total electron density at the saddle critical points along the bonds are given in Table 4. The only difference with respect to the Mulliken analysis involves the H_1-Pd_1 bond: according to the Bader analysis, this bond is stronger in the HF calculation than in the DF one. In Figure 9 the (3,3) critical point, an absolute minimum in the total electron density, which is a characteristic feature of three-center bonds, is clearly evident at the center of the $P_2-H_1-Pd_1$ triangle.

(e) The introduction of the H^+ ion weakens the P−M bonds, except for P_1-Pt_1 and P_3-M_2, thereby accounting for the absence of a trans effect of the hydride ligand.[20]

(f) From the Mulliken analysis, the Pt_1-Pt_2 interaction is stronger than the Pd_1-Pd_2 one, and is especially enhanced by the inclusion of electron correlation, whereas this is negligible at the HF level in the related conjugate bases. However, these results were not entirely confirmed by a Bader analysis.[25] We do not show all the corresponding plots here, but we report the values of the total electron density (in a.u.) at the saddle critical point along the M_1-M_2 bond at the HF (and DF) level: ρ(Pd−Pd) = 0.0498 (0.0509) for **4**$^+$, ρ(Pt−Pt) = 0.0750 (0.0733) for **2**$^+$, and ρ(Pd−Pd) = 0.0501 (0.0509), ρ(Pt−Pt) = 0.0642 (0.0649) for the respective conjugate bases. These values show that an appreciable M_1-M_2 bond is present in both **2**$^+$ and **4**$^+$ and their related neutral compounds, that the inclusion of electron correlation does not significantly alter such a bond, and finally that the Pt−Pt bond is stronger than the Pd−Pd one and is further strengthened by protonation, whereas the Pd−Pd bond is not affected. In other words, the Pt−Pt system reacts to the introduction of the H^+ ion by drawing charge from the external region of the complex and by accumulating it on the Pt_1 center, resulting finally in a situation in which Pt_1 is more negative and the Pt−Pt bond is stronger than in the related neutral compound. In the Pd case, the final situation is nearly identical to the original one, in good agreement with the X-ray Pd−Pd bond distances in **4**$^+$ and its conjugate base, which were found to be 2.611(1) and 2.594(1) Å, respectively;[14] the small difference of 0.017 Å may be due to packing effects. Since X-ray data for [Pt(μ-PBu$^t_2$)(PBu$^t_2$H)]$_2$ are not yet available, an experimental confirmation for the platinum systems is not possible; however, metal−metal bond-shortening induced by protonation, although uncommon, has been observed.[26]

As a final confirmation of the above analysis, the second derivatives of the energy with respect to the H_1 coordinates at the four minima have been evaluated, the corresponding Hessian matrixes have been diagonalized, and the vibrational eigenvalues and eigenvectors have been calculated. From these HF (and DF) calculations, one finds that the H_1 atom exhibits an H−Pt stretching mode at ν = 1985 (1817) cm^{-1} and two bending modes at ν = 878 (899) cm^{-1} and 427 (334) cm^{-1}. In the Pd case in contrast, one finds two modes at ν = 1602 (1374) cm^{-1} and 1264 (997) cm^{-1} and one bending mode at ν = 889 (511) cm^{-1}. The three modes are strongly mixed in the DF calculations, further confirming the three-center nature of the bonding

(25) The partial disagreement between the Mulliken and Bader analyses reminds one of the limitations of the former: Its results must always be taken with some caution but are seldom completely contradicted by more sophisticated approaches, especially where trends and differences between related compounds are concerned.

(26) Elliot, D. J.; Vittal, J. J.; Puddephatt, R. J.; Holah, D. G. and Hughes, A. N. *Inorg. Chem.* **1992**, *31*, 1247.

situation. The $\nu = 1985$ (1819) cm^{-1} stretching mode in the Pt case is in fair agreement with the IR measurements of an active mode at 2039 cm^{-1}, whereas the two in-plane modes in the Pd case are probably obscured by the strong C−C and C−P absorptions, particularly if the DF values are taken. In this context, a full account of relativistic effects for the Pt atom would strengthen the H−Pt bond,[24] which, at variance with usual findings, makes the HF values closer to the experimental results than the DF ones.

In conclusion, the ab initio analysis strongly supports the suggestion of NMR and chemical analysis, showing a picture of P−H−M interactions that is in full agreement with the experimental data.

Experimental Section

General Data. All reactions were carried out under a nitrogen atmosphere, by using standard Schlenk techniques. $[Cp_2Fe]PF_6$[27] and $[Pt(\mu\text{-}PBu^t_2)(H)(PBu^t_2H)]_2$, **1**,[13] were prepared as previously described; TCNE (Aldrich) and TCNQ (Aldrich) were recrystallized twice from toluene; Et_3N (Aldrich) was used as purchased. Solvents were dried by conventional methods and distilled under nitrogen prior to use. IR spectra (Nujol mulls, KBr) were recorded with a Perkin-Elmer Fourier transform IR 1725X spectrophotometer. NMR spectra were recorded with a Varian Gemini 200 BB instrument; frequencies are referenced to Me_4Si (^1H), 85% H_3PO_4 (^{31}P), and H_2PtCl_6 (^{195}Pt). Solid-state NMR spectra were recorded with a Bruker AMX 300-WB instrument equipped with a CP/MAS probe using 4 mm rotors. The lack of hydrogen evolution was detected by gas-chromatographic analyses performed with a DANI 3200 instrument equipped with a D-SM 5A column. Magnetic susceptibility measurements were performed with a Faraday balance standardized with $CuSO_4 \cdot 5H_2O$; Pascal contributions[28] were used.

Preparation of 1·(TCNE). The colorless complex **1**, (300 mg, 0.308 mmol) was suspended in a 20-mL solution of TCNE (42 mg, 0.328 mmol) in toluene, and a deep violet solid was formed immediately. This air-sensitive insoluble solid was filtered, washed with toluene (5 mL) and vacuum dried (245 mg, 0.222 mmol, 72% yield). Elem. Anal. Calcd. for $C_{38}H_{76}N_4P_4Pt_2$: C, 41.4; H, 6.94; N, 5.08. Found: C, 40.9; H, 6.78; N, 4.83. IR (Nujol, KBr): 2289 (ν_{PH}), 2189, 2174, 2161 and 2145 (ν_{CN}), 2031 (ν_{PtH}) cm^{-1}. $\mu_{eff} = 1.46\ \mu_B$. The solid is completely insoluble in nonpolar solvents and decomposes in polar solvents; therefore only solid-state analyses were carried out.

Preparation of 2a. Complex **1** (188 mg, 0.193 mmol) was suspended in a 20-mL solution of TCNE (50 mg, 0.390 mmol) in THF. The suspension turned immediately deep red, while the solid slowly dissolved (15 min), giving an orange solution. Gas-chromatographic analysis of the gas-phase did not reveal the presence of H_2. Most of the solvent was evaporated and the addition of Et_2O (5 mL) induced the precipitation of **2a** as an orange microcrystalline solid. The latter was filtered, washed with Et_2O (5 mL), and vacuum dried (175 mg, 0.159 mmol, 82% yield). Elem. Anal. Calcd. for $C_{38}H_{75}N_4P_4Pt_2$: C, 41.4; H, 6.86; N, 5.08. Found: C, 40.8; H, 6.82; N, 4.95. IR (Nujol, KBr): 2360 (w), 2341 (w) (ν_{PH}), 2188, 2159 (ν_{CN}), 2040 (w) (ν_{PtH}) cm^{-1}. UV−Vis (CH_3CN, 298 K): 23375 cm^{-1} (broad absorption with vibrational overtones).[10] $\mu_{eff} = 1.62\ \mu_B$. See the table shown in Figure 3 for NMR parameters.

Crystals of **2b** suitable for the X-ray analysis were obtained by slow evaporation in air of an acetone/Et_2O solution of complex **2a**.

Preparation of 2c. TCNQ (36 mg, 0.176 mmol) was added to a suspension of complex **1** (86 mg, 0.088 mmol) in toluene (10 mL). A deep green solution formed within a few minutes, and **2c** precipitated out as a microcrystalline deep green solid. The solid was filtered, washed with *n*-hexane (5 mL), and vacuum dried, yielding 80 mg (0.0679 mmol, 77% yield). Elem. Anal. Calcd. for $C_{44}H_{79}N_4P_4Pt_2$: C, 44.9; H, 6.76; N, 4.75. Found: C, 43.9; H, 6.71; N, 4.66. $^{31}P\{^1H\}$, ^{31}P and ^1H NMR spectra were superimposable to the corresponding spectra of $(\mathbf{2})^+TCNE^-$. $\mu_{eff} = 1.82\ \mu_B$.

Reaction of 1 with $[Cp_2Fe]PF_6$. Method A: Complex **1** (97 mg, 0.0995 mmol) and an equimolar amount of $[Cp_2Fe]PF_6$ (33 mg) were suspended in toluene (15 mL) and stirred for 4 h at 50 °C. The solids slowly dissolved, leaving an orange solution that was shown ($^{31}P\{^1H\}$ NMR) to contain only a 1/1 mixture of (**2**)PF_6, **2d**, and (**3**)PF_6. The solution was kept overnight at −30 °C, and an orange powder, containing the same ratio of the complexes, precipitated out and was filtered and vacuum dried (61 mg).

Method B: Complex **1** (163 mg, 0.167 mmol) and a twofold excess of $[Cp_2Fe]PF_6$ (111 mg) were suspended in toluene (20 mL). Et_3N (0.07 mL, 0.502 mmol) was added and the suspension was stirred for 4 h at 50 °C. The orange solution resulting was kept overnight at −30 °C, allowing an orange powder to precipitate out. This powder was filtered, washed with *n*-hexane, and vacuum dried. The solid was then dissolved in CH_2Cl_2 (10 mL) and $[Et_3NH]PF_6$ was filtered off. The solution was concentrated to a small volume (~2 mL), and Et_2O (15 mL) was added, yielding **2d** as an orange microcrystalline solid (163 mg, 0.146 mmol, 87% yield). Elem. Anal. Calcd. for $C_{32}H_{75}F_6P_5Pt_2$: C, 34.3; H, 6.76. Found: C, 34.6; H, 6.72. ^1H and ^{31}P NMR spectra were identical to the corresponding spectra of **2a**−**c**, except for an added septet at −139 ppm ($^1J_{PF} = 708$ Hz) in the $^{31}P\{^1H\}$ NMR spectrum. IR (Nujol, KBr): 2359 (w), 2342 (w) (ν_{PH}), 2039 (w) (ν_{PtH}), 839 (vs) (ν_{PF}) cm^{-1}. Diamagnetic.

Crystallography. Single crystals of **2b** suitable for X-ray diffraction were obtained as described above; for **2c** we were only able to obtain crystals of poor quality from acetone/Et_2O mixtures.

Crystals of both compounds were mounted on glass fibers, on a CAD4 diffractometer, that was used for the space group determination and for the data collection. Unit cell dimensions were obtained by least-squares fit of the 2θ values of 25 high-order reflections. Crystallographic and other relevant data are listed in Table 5 and Supplementary Table S1. Data were measured with variable scan speed to ensure constant statistical precision on the collected intensities. Three standard reflections, used to check the stability of the crystals and of the experimental conditions, were measured every hour. The collected intensities were corrected for Lorentz and polarization factors.

Table 5. Crystallographic and Experimental Data for the X-ray Diffraction Study of **2b** and **2c**

compound	**2b**	**2c**
formula	$C_{40}H_{75}N_5P_4Pt_2$	$C_{44}H_{78}N_4P_4Pt_2$
fw	1140.15	1177.22
crystal dimens, mm	0.4 × 0.3 × 0.3	0.5 × 0.4 × 0.3
data collect *T*, °C	23	23
crystal system	monoclinic	triclinic
space group	*P2₁* (no. 4)	*P-1* (no. 2)
a, Å	19.528 (7)	9.159 (11)
b, Å	12.267 (4)	11.462 (8)
c, Å	20.649 (2)	13.621 (13)
α, °	90.	71.43 (9)
β, °	98.95 (2)	83.26 (10)
γ, °	90.	69.60 (8)
V, Å^3	4895 (2)	1269 (3)
Z	4	1
ρ_{calcd}, g cm^{-3}	1.553	1.537
radiation	Mo Kα (graphite monochrom. $\lambda = 0.71069$ Å)	
μ, cm^{-1}	59.507	57.071
transmission coeff	0.9998−0.8614	1.1936−0.6708
θ range, °	$2.5 < \theta < 25.0$	$2.5 < \theta < 25.0$
no. of unique reflecns	6249	4801
no. of obs reflectns, n_o	4783 [$\lvert F_o\rvert > 3.0\sigma(\lvert F\rvert)$]	3388 [$\lvert F_o\rvert > 4.5\sigma(\lvert F\rvert)$]
R	0.042	0.073
R_w	0.061	0.101

[a] $R = \sum(|F_o - (1/k)F_c|)/\sum|F_o|$ and $R_w = [\sum_w(F_o - (1/k)F_c)^2/\sum_w|F_o|^2]^{1/2}$, where: $w = [\sigma^2(F_o)]^{-1}$, $\sigma(F_o) = [\sigma^2(F_o^2) + f^4(F_o^2)]^{1/2}/2F_o$, and $f = 0.050$.

(27) Brauer, G. In *Handbuch der Präparativen Anorganischen Chemie*; Ferdinand Enke Verlag: Stuttgart, 1981; p 1845.

(28) The diamagnetic contributions are from König, E. Magnetische Eigenschaften der Koordinations- und Metallorganischen Verbindungen der Übergangselemente. In *Landolt-Börnstein, Zahlenwerte und Funktionen aus Naturwissenschaften und Technik*; Springer-Verlag: Berlin, 1966; 6th ed., Vol. 2, p 16.

The standard deviations of intensities were calculated in terms of statistics alone, while those on F_o were calculated as shown in Table 5.

The structures were solved by a combination of Patterson and Fourier methods and refined by full matrix least-squares[29] (the function minimized being $\sum[w(F_o - 1/k\ F_c)^2]$).

The refinements were carried, for the two compounds, in the centrosymmetric space groups P-1 and *C*2/*c*, respectively.

In an attempt to show the expected asymmetry of the coordination around the Pt atoms, compounds **2b** and **2c** were also refined in the corresponding noncentrosymmetric space groups (P1 and Cc, respectively) to remove the pseudosymmetry imposed in the centrosymmetric space groups.

These attempts lead to agreement factors that were not significantly better[30] than the centrosymmetric model but called for a greater spread of the bond lengths and angles. Therefore the centrosymmetric model, with fewer parameters, was retained in both cases.

No extinction correction was deemed necessary. The scattering factors used, corrected for the real and imaginary parts of the anomalous dispersion, were taken from the literature.[30]

The contribution of the hydrogen atoms in calculated positions, i.e., C−H = 0.95 (Å), B(H) = 1.3 × B(C_{bonded})(Å^2), was taken into account but not refined. Upon convergence (see Supporting Information, Table S1) no significant features were found in the Fourier difference maps of both compounds.

Final agreement factors and other relevant data for the refinement are given in Table 5. All calculations were carried out by using the Enraf-Nonius MOLEN package.[29]

Structural Study of 2b. An empirical absorption correction[31] was applied to the data set by using azimuthal (Ψ) scans of three "high-χ" (χ > 85°) reflections. Of the 6249 independent data collected, 4801 were considered as observed and used for the refinement. The final full matrix least-squares refinement cycles were carried out by using anisotropic displacement parameters for all atoms.

The $[C_3(CN)_5]^-$ showed signs of being disordered, as can be judged from the values of the displacement parameters and the spread of the C−N distances. However, no meaningful model (with split positions for some of the atoms) could be refined.

Structural Study of 2c. As mentioned above, only crystals of very unsatisfactory quality could be obtained for this complex. Eventually a crystal was found that, although split, gave diffraction peaks that were separated enough to allow unambiguous indexing and data collection. The resulting quality of the structure determination is, however, limited [note the high standard deviations of the refined parameters].

A total of 4783 independent reflections were collected, of which only 3388 were observed [$F_o > 4.5\sigma$ (F)] and used for the refinement.

Because the crystal was not single, we were unable to correct for absorption by using azimuthal (Ψ) scans; thus, when the final model was obtained, we applied the DIFABS procedure.[32]

The structure was refined as described above, with use of anisotropic displacement parameters for the platinum, phosphorus, and nitrogen atoms; all other atoms were treated isotropically. No significant improvement in the model[33] was obtained by increasing the number of refined parameters.

Computational Details

The ab initio HF and DF calculations were performed with the GAUSSIAN 94[34] set of programs. The standard double-ζ quality LanL2DZ[35] basis set was used, which utilizes pseudopotentials and incorporates spin−orbit averaged relativistic effects for the Pt atom. Despite the lack of polarization functions in the basis set and of Darwin and mass-polarization relativistic corrections in the pseudopotentials, the present computational approach usually describes in a reasonable way the energetics of the Pt−H, Pt−P, and P−H bonds. The Bader population analysis,[23] not supported by GAUSSIAN 94, was performed at the simplest possible level by locating the critical points of the total electron density through direct inspection of plots in the P−H−M plane.

Acknowledgment. Italian Consiglio Nazionale delle Ricerche (CNR) and Ministero dell'Università e della Ricerca Scientifica e Tecnologica (MURST) are gratefully acknowledged for financial support. Claudia Forte is gratefully acknowledged for experienced assistance in doing and interpreting the solid-state NMR spectra.

Supporting Information Available: A detailed analysis of the ^{1}H, ^{31}P, and ^{195}Pt NMR spectra of complex **2a**; a full listing of crystallographic data for **2b** and **2c**, including tables of positional and isotropic equivalent displacement parameters, calculated positions of the hydrogen atoms, anisotropic displacement parameters, bond distances, and angles; ORTEP figures showing the full numbering schemes (19 pages, print/PDF). See any current masthead page for ordering information and Web access instructions.

JA980932R

(29) *MOLEN: Molecular Structure Solution Procedure*; Enraf-Nonius: Delft, The Netherlands, 1990.

(30) Cromer, D. T.; Waber, J. T. In *International Tables for X-ray Crystallography*; Kynoch: Birmingham: England, 1974; Vol. IV.

(31) North, A. C. T.; Philips, D. C.; Mathews, F. S. *Acta Crystallogr.* **1968**, *A24*, 351.

(32) Walker, N.; Stuart, D. *Acta Crystallogr. Sect. A* **1983,** *39*, 159.

(33) Hamilton, W. C. *Acta Cristallogr.* **1965**, *17*, 502.

(34) Frisch, M. J.; Trucks, G. W.; Schlegel, H. B.; Gill, P. M. W.; Johnson, B. G.; Robb, M. A.; Cheeseman, J. R.; Keith, T.; Petersson, G. A.; Montgomery, J. A.; Raghavachari, K.; Al-Laham, M. A.; Zakrzewski, V. G.; Ortiz, J. V.; Foresman, J. B.; Cioslowski, J.; Stefanov, B. B.; Nanayakkara, A.; Challacombe, M.; Peng, C. Y.; Ayala, P. Y.; Chen, W.; Wong, M. W.; Andres, J. L.; Replogle, E. S.; Gomperts, R.; Martin, R. L.; Fox, D. J.; Binkley, J. S.; Defrees, D. J.; Baker, J.; Stewart, J. P.; Head-Gordon, M.; Gonzalez, C.; Pople, J. A. *Gaussian 94, Revisions B.3 and D.4*, Gaussian, Inc.: Pittsburgh, PA, 1995.

(35) (a) Hay, P. J.; Wadt, W. R. *J. Chem. Phys.* **1985**, *82*, 270. (b) Wadt, W. R.; Hay, P. J. *J. Chem. Phys.* **1985**, *82*, 284. (c) Hay, P. J.; Wadt, W. R. *J. Chem. Phys.* **1985**, *82*, 299.